Geomorphology 105 (2009) 322–333

Contents lists available at ScienceDirect

Geomorphology

journal homepage: www.elsevier.com/locate/geomorph

Controls on the height and spacing of eolian ripples and transverse dunes: A numerical modeling investigation

Jon D. Pelletier

Department of Geosciences, The University of Arizona, 1040 E. Fourth St., Tucson, Arizona, 85721, USA

ARTICLE INFO

Article history:
Received 14 June 2008
Received in revised form 14 October 2008
Accepted 16 October 2008
Available online 28 October 2008

Keywords:
Eolian geomorphology
Ripples
Dunes
Numerical modeling

ABSTRACT

Ripples and transverse dunes in areas of abundant sand supply increase in height and spacing as a function of time, grain size, and excess shear velocity. How and why each of these factors influence ripple and transverse dune size, however, is not precisely known. In this paper, the controls on the height and spacing of ripples and transverse dunes in areas of abundant sand supply are investigated using a numerical model for the formation of eolian bedforms from an initially flat surface. This bedform evolution model combines the basic elements of Werner's [Werner, B.T., 1995. Eolian dunes: Computer simulations and attractor interpretation. Geology 23, 1107–1110.] cellular automaton model of dune formation with a model for boundary layer flow over complex topography. Particular attention is paid to the relationship between bed shear stress and slope on the windward (stoss) side of evolving bedforms. Nonlinear boundary layer model results indicate that bed shear stresses on stoss slopes increase with increasing slope angle up to approximately 20°, then decrease with increasing slope angle as backpressure effects become limiting. In the bedform evolution model, the linear boundary layer flow model of Jackson and Hunt [Jackson, P.S., Hunt, J.C.R., 1975. Turbulent wind flow over a low hill. Quarterly Journal of the Royal Meteorological Society 101, 929–955.], generalized to 3D, is modified to include the nonlinear relationship between bed shear stress and slope. Bed shear stresses predicted by the modified Jackson and Hunt flow model are then used to predict rates of erosion and deposition iteratively through time within a mass-conservative framework similar to Werner [Werner, B.T., 1995. Eolian dunes: Computer simulations and attractor interpretation. Geology 23, 1107–1110.]. Beginning with a flat bed, the model forms ripples that grow in height and spacing until a dynamic steady-state condition is achieved in which bedforms migrate downwind without further growth. The steady-state ripple spacing predicted by this model is approximately 3000 times greater than the aerodynamic roughness length of the initially flat surface, which is a function of grain size and excess shear velocity. Once steady-state ripples form, they become the dominant roughness element of the surface. The increase in roughness associated with ripple formation triggers the same bedform instability that created ripples, causing dunes to form at a larger scale. In this way, the numerical model of this paper suggests that ripples and dunes are genetically linked. Transverse dunes in this model have a steady-state height and spacing that is controlled by the effective roughness length of the rippled surface, which is shown to be on the order of 500 times greater than the original roughness length, but varies significantly with the details of ripple morphology. The model predictions for ripple and dune spacing and their controlling variables are consistent with field measurements from the published literature. The model of this paper provides a preliminary process-based understanding of the granulometric control of ripples and dunes in areas of abundant sand supply and unidirectional prevailing winds, and it argues for a genetic linkage between ripples and dunes via a scaling relationship between eolian bedform size and the aerodynamic roughness length.

1. Introduction

1.1. Problem statement

Eolian bedforms are constructed by a positive feedback in which incipient, small-amplitude perturbations modify the air flow around them to cause spatial variations in erosion and deposition that promote taller and more widely-spaced bedforms over time. How this process works at small (ripple) and large (dune) scales, however, is still not well understood and a number of questions remain. First, field measurements indicate that the height and spacing of ripples are positively correlated with grain size and excess shear velocity (Sharp, 1963; Walker, 1981) and that the height and spacing of transverse dunes are also positively correlated with grain size in areas of abundant sand supply (Wilson, 1972; Lancaster, 1988). How and why these factors influence bedform size, however, is not precisely known. Moreover, it is still unclear whether dunes grow in size indefinitely, or

E-mail address: jon@geo.arizona.edu.

0169-555X/$ – see front matter © 2008 Elsevier B.V. All rights reserved.
doi:10.1016/j.geomorph.2008.10.010

whether, after an initial period of growth, they achieve a dynamic steady-state condition in which they migrate downwind without further growth. In this paper we take a numerical modeling approach to addressing these questions, integrating the cellular automaton model of Werner (1995) with a realistic boundary layer flow model in order to investigate the coupling between boundary layer flow and bedform evolution at both small and large scales. The model results suggest that boundary layer flow processes set a limit on bedform size.

In this paper, I describe a process-based numerical model designed to determine the controls on the height and spacing of ripples and dunes. The model combines the strengths of the Werner (1995) model framework, which successfully generates self-organized bedforms from an initially-flat surface, with the Schwammle and Herrmann (2004) framework, which successfully quantifies the positive feedback between topography, air flow, and erosion/deposition during bedform evolution. In this paper I focus on the simplest case of ripple and dune development in areas of abundant sand supply (i.e. 100% sand cover). Also, the model assumes unidirectional winds and does not explicitly include variable grain sizes or sorting effects. In focusing on this simple, idealized case, it is not my intention to imply that the effects of limited sand supply, shifting winds, and/or spatial and temporal variations in grain size are unimportant in natural dunes. Rather, my goal is to understand the coupling between boundary layer flow and bedform evolution for this simple case first before adding additional complexity.

1.2. Field and remote-sensing observations

There are three fundamental types of transverse eolian bedforms that form in areas of abundant sand supply and unidirectional prevailing winds. Ripples occur at the smallest scale and are typically spaced from 0.01–10 m and have heights of 0.2–50 cm, with higher, more widely-spaced ripples forming in areas with stronger winds and/or coarser sand (Sharp, 1963; Wilson, 1972). Dunes are the next level in the bedform hierarchy and achieve spacings of 10–1000 m and heights of 0.5–50 m. At still larger scales, megadunes may form and reach heights of 50–300 m and spacings of 1–3 km, given sufficient time in addition to sand supply. Working in the large sand seas of the Sahara Desert, Wilson (1972) documented a positive correlation between the grain diameter of the coarsest twentieth percentile of crestal sand and the height and spacing of each bedform type (Fig. 1). Working in the Skeleton Coast, Namib, and Gran Desierto sand seas, Lancaster (1988) documented a correlation between dune spacing and grain size in compound crescentic (i.e. transverse) dunes. The spacing of barchan, star, and longitudinal dunes in Lancaster's study areas did not show any correlation with grain size.

One way that grain size may affect the size of ripples and dunes is via the aerodynamic roughness length. The aerodynamic "law of the wall" states that the wind velocity profile above a rough surface is a function of the aerodynamic roughness length, which, during saltation, is a function of both grain size and excess shear velocity (Sherman, 1992). Therefore, if the spacing of bedforms is controlled in a significant way by the wind velocity profile above the bed, it is reasonable to hypothesize that the size of bedforms will be partially controlled by grain size and excess shear velocity. This is the fundamental hypothesis investigated in this paper.

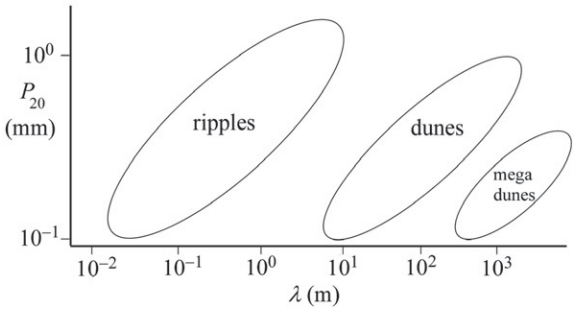

Fig. 1. Schematic plot of grain diameter of coarsest twentieth percentile crestal sand, P_{20}, and bedform spacing, λ, from transverse eolian bedforms of the Sahara Sand Seas. After Wilson (1972).

In ripples, spacing is well established to increase with increasing grain size and excess shear velocity (Sharp, 1963; Walker, 1981; Andreotti et al., 2006), although there is still no process-based understanding of how those variables control spacing. Bagnold (1941) performed the pioneering work on the height and spacing of eolian ripples. He proposed that ripples form by an instability mechanism in which a small, incipient perturbation in the bed topography exposes the windward side to more impacts and faster surface creep than the leeward side, resulting in more grains being ejected into saltation. In his theory, sand grains move a characteristic saltation distance, resulting in periodic ripples with spacing equal to that characteristic distance. The fact that ripple spacing increases over time in both field and laboratory experiments (Sharp, 1963; Seppala and Linde, 1978; Walker, 1981), however, is inconsistent with Bagnold's concept of a constant characteristic saltation length. Moreover, experimental studies of grain impacts suggest that a wide distribution of energies are imparted to grains on the bed during each impact, resulting in a wide distribution of saltation path lengths (Mitha et al., 1986). Using a discrete particle framework informed by Mitha et al.'s (1986) work, Anderson (1987) and Anderson and Bunas (1993) constructed models for ripple formation and evolution aimed at understanding the controls on ripple height and spacing. Anderson (1987) argued that ripple spacing is controlled by the mean reputation length. Anderson's model is a linear-stability analysis, however, and hence only addresses the spacing of ripples early on in their development from a flat surface. Anderson and Bunas (1993) modeled the evolution of ripples using the distribution of particle paths documented by Mitha et al. (1986), together with a simplified boundary layer flow model. In their model, ripples grow in height and spacing until a steady-state condition is achieved. The steady-state behavior in their model, however, was directly related to an arbitrary "ceiling" imposed on the flow in their model. As a result, there is currently no realistic model for ripples that predicts a steady-state relationship between grain size and excess shear velocity control ripple size, as observed.

The controls on the spacing of dunes are also incompletely understood. As noted above, Wilson (1972) and Lancaster (1988) both documented positive correlations between grain size and dune height and dune spacing. On the other hand, tests of granulometric control of bedform height and spacing in barchan, star, and longitudinal dunes all show no grain size control (e.g. Wasson and Hyde, 1983; Lancaster, 1988; Ould Ahmedou et al., 2007; Elbelrhiti et al., 2008). It is important to distinguish between dunes formed in areas of abundant sand supply from those formed in areas of limited sand supply in this context, however. In areas of limited sand supply (i.e. partial sand cover), the aerodynamic roughness length will be at least partially controlled by the roughness elements (e.g. vegetation, alluvial deposits, and bedrock outcrops) that comprise the interdune or sand-free areas. As the percent of sand cover decreases significantly below 100% in a dune field, the aerodynamic roughness length will become progressively more influenced by the size of the roughness elements in the interdune areas (which generally have no relationship with the grain size of sand on the dunes). For this reason, the height and spacing of barchan, star, and longitudinal dunes are not likely to exhibit granulometric control, even if the boundary layer flow over these types of dunes exerts a controlling influence on their morphology. For this reason, we will not consider those dune types in this paper.

Most conceptual models for eolian dune formation relate dune height and spacing to the dimensions of the zone of disturbance downwind (e.g. Hanna, 1969; Wilson, 1972; Folk, 1976). It is difficult to

separate cause and effect in these conceptual models, however, because, it is unclear whether the size of the zone of separation controls, or is controlled by, dune size. Moreover, the size of the zone of separation is controlled by other parameters besides dune size and shape in ways that have not been fully quantified. For example, Howard et al. (1989) proposed that dune size is controlled, in part, by the aerodynamic roughness length upwind because it is this length scale that determines the speedup ratio on the windward size of dunes for a given dune height and aspect ratio. How the aerodynamic roughness length influences dune size, however, is still uncertain. Indeed, whether dune size is controlled primarily by the characteristics of boundary layer flow (e.g. Howard et al., 1989; Schwammle and Herrmann, 2004) or by the nonlinear dynamics intrinsic to interacting bedforms (e.g. Werner and Gillespie, 1993; Werner and Kocurek, 1999) is still debated.

1.3. Previous process-based modeling work

Werner (1995) was the first to model the formation of eolian dunes numerically from an initially flat surface. Werner's (1995) model is based on the iterative entrainment, transport, and deposition of discrete units of sand that are picked up at random, transported multiples of a characteristic distance downwind, and redeposited back onto the surface. Sand units transported by the model during a given iteration are deposited on the bed with a probability that is low on bedrock surfaces relative to sandy surfaces (reflecting the higher coefficient of restitution of a hard bed versus a soft bed). Sand units that are not deposited are transported repeatedly downwind until deposition occurs. In this way, the local sand flux above the surface is directly proportional to the probability of deposition. In Werner's model, the effect of air flow over incipient dunes is included in a simplified way by defining "shadow" zones where the probability of deposition is one. Shadow zones are defined to be areas located in shadow when the surface is illuminated by a sun angle of 15° from the horizontal and parallel to the wind direction. In Werner's model, shadow zones provide a simplified representation of the recirculation zone on the lee sides of incipient dunes where wind-driven sediment flux is low and deposition rates are high. Sand units deposited back down on the bed in Werner's model roll down the direction of steepest descent if deposition causes an oversteepened condition (i.e. a slope angle greater than the angle of repose). Werner's model combines three basic elements that, taken together, are responsible for the complex self-organized behavior observed in the model. First, the stochastic model of entrainment generates initially structureless, multi-scale relief from an initially flat bed. Second, shadow zones provide a mechanism for a positive feedback between the topography of incipient bedforms and the spatial pattern of erosion and deposition that enhances bedform height and spacing over time. Finally, avalanching provides a limitation on dune slope and a mechanism for cross-wind sand transport. Example output of Werner's model is illustrated in Fig. 2. The height and spacing of bedforms in Werner's model increase proportionately to the square root of time until a single dune, equivalent in size to the model domain, remains.

Werner's model is capable of reproducing the four principal dune types (transverse, barchan, star, and longitudinal) by varying sand supply and wind direction variability. Despite the success of Werner's model for understanding dune types, the model has limitations for understanding dune size. Werner's model includes the physics of boundary layer flow over topography only in a very limited way. For example, erosion on the stoss side of evolving bedforms is independent of both height and slope in Werner's model, an assumption that is inconsistent with basic field measurements (Lancaster, 1996). Werner's model also predicts symmetric topographic profiles when bedforms evolve in a unidirectional wind regime, while bedform profiles in nature are asymmetric under unidirectional wind conditions. Momiji et al. (2000) constructed a modified version of Werner's model capable of producing asymmetric bedforms by prescribing erosion on the windward side of bedforms to be a nonlinear function of slope. Nevertheless, both of these models have no prescribed length scale and they depend on parameters that are abstracted from the actual transport processes (e.g. saltation). As such, they are difficult to calibrate for comparison to real-world bedforms (Baas, 2007).

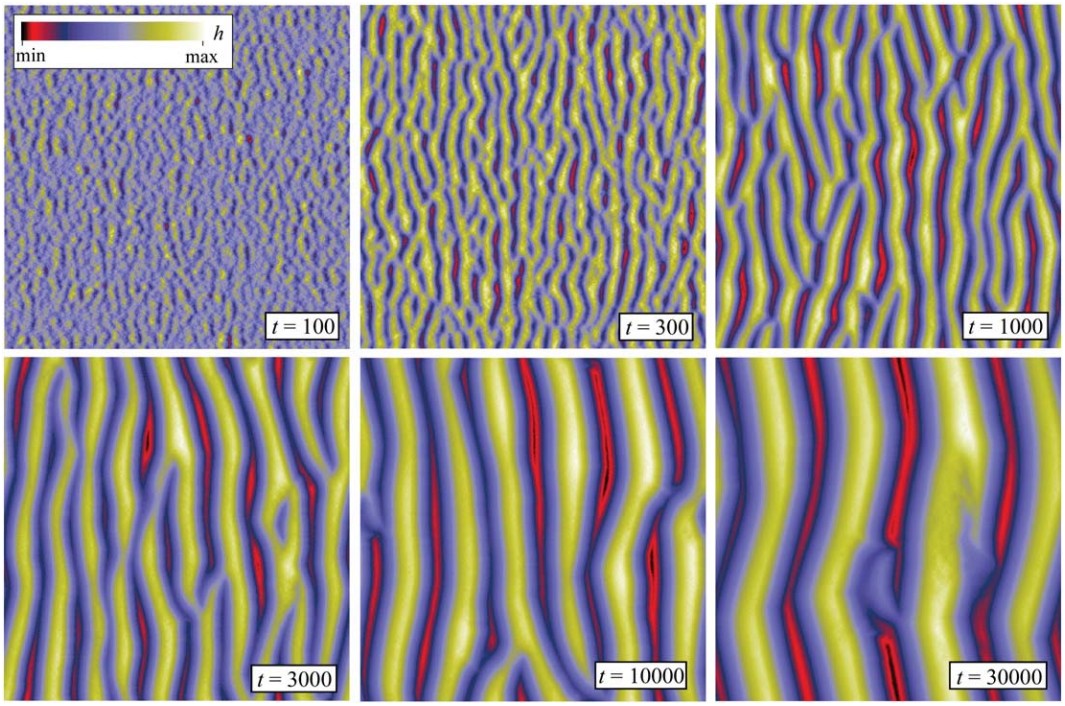

Fig. 2. Color maps of elevation predicted by Werner's model for dunes at t=100, 300, 1000, 3000, 10,000, and 30,000 ($\times N^2$) time steps. Wind direction is from left to right. In the model, dune height and spacing increase proportionately to the square root of time until only one dune remains, equivalent in size to the model domain. Note that each color map is separately scaled so that black is the minimum height and white is the maximum.

Following upon Werner's work, Stam (1996, 1997), Van Dijk et al. (1999), and Schwammle and Herrmann (2004) developed numerical models that include the physics of boundary layer flow over evolving transverse bedforms. These models, in turn, followed upon an earlier generation of boundary layer flow models over barchan dunes (e.g. Wippermann and Gross, 1986). Stam's (1996, 1997) model was limited to 2D and could not be used to model the evolution of dunes from an initially flat bed (i.e. Stam's model predicted that the smallest wavelengths were the most unstable, leading to infinitely steep slopes). Given that the height and spacing of dunes depends on the interaction of bedforms and defects in 3D (e.g. Werner and Kocurek, 1999), it is unlikely that any 2D model will be sufficient to determine the controls on bedform height and spacing. In Van Dijk et al.'s (1999) and Schwammle and Herrmann's (2004) models, sine waves and small Gaussian hills were used as an initial conditions, respectively. As such, these models do not simulate bedform evolution from a structureless initial condition and hence they do not directly constrain the height and spacing of natural bedforms. Moreover, because both models require a characteristic bedform length L to be input into the model, the size of the bedforms produced by these models is, to some extent, prescribed by the input data. A comprehensive model of bedforms must predict bedform lengths rather than input them into the model.

All of the bedform evolution models that include boundary layer flow have used the Jackson and Hunt (1975) boundary layer model for flow over "low" hills as their foundation (later generalized to 3D by Mason and Sykes, 1979). This model, as well as subsequent Fourier-Transform-based models for boundary layer flow (i.e. Weng et al., 1991), solve the linearized Reynolds stress equations over prescribed bed topography. Boundary-layer models based on linearized Fourier-Transform techniques have the advantage of computational speed, thus allowing them to be integrated into bedform evolution models that require bed shear stresses to be calculated during each model time step for tens of thousands of time steps. More sophisticated computational fluid dynamics models (i.e. Large Eddy Simulation (LES) and Direct Numerical Simulation (DNS) methods) have the advantage of greater accuracy than linearized Reynolds' stress models, but they are too computationally intensive to be run for the tens of thousands of iterations required by bedform evolution models. Linearized Reynolds' stress models such as the Jackson and Hunt model do not adequately compute the stresses over steep ($>10°$) bedforms, however. As such, these models must be modified to account for nonlinear flow effects over steep topography. Schwammle and Herrmann (2004), for example, incorporated the effects of flow separation over the lee sides of growing dunes by correcting a linearized Reynolds' stress model solution using a geometric model for the separation zone. Flow separation, however, affects the entire wind field, not just the zone of separation, hence a local correction does not fully account for the effects of nonlinear flow processes on bed shear stresses and erosion rates on the stoss sides of evolving bedforms.

Recent work has suggested that bedform spacing is controlled by the evolution of defects in bedform populations over time (Werner and Gillespie, 1993; Werner and Kocurek, 1997, 1999). The defect density model predicts that bedform height and spacing grows linearly with time from an initial value, then transitions to a logarithmic increase in time. While defect density and bedform spacing are strongly correlated during bedform development (suggesting that defect density directly controls height and spacing), it should be noted that this model makes a number of simplifying assumptions (e.g. bedforms are uniformly spaced and of uniform height, aerodynamics plays no role in bedform migration, and defects are not created over time). The defect density model is also limited in that it requires input data for the initial bedform spacing. This value largely determines the final bedform spacing predicted by the model.

2. Numerical modeling

2.1. Model description

At the start of each iteration of the model, the topography $h(x,y)$ is used as input to a boundary layer flow model that calculates the bed shear stresses over complex topography. This boundary-layer model is a 3D version of the Jackson and Hunt (J&H) (1975) model for flow over low hills, modified to include the nonlinear effects of flow over steep topography. Bed shear stress in the J&H model, τ_b, can be written as the sum of the shear stress over flat topography, τ_{b0}, plus the normalized variation in bed shear stress induced by the variations in topography, τ_{b1}:

$$\tau_b = \tau_{b0}(1+\tau_{b1}). \tag{1}$$

According to the J&H model, the Fourier Transform of the normalized variations in bed shear stress, $\hat{\tau}_{b1,}$ is given by x and y components:

$$\hat{\tau}_{b1x}(k_x,k_y) = \varepsilon\kappa\frac{k_x^2}{|k|}\hat{h}(k_x,k_y)z_k\frac{K_1(z_k e^{i\varphi})}{K_0(z_k e^{i\varphi})}, \tag{2}$$

$$\hat{\tau}_{b1y}(k_x,k_y) = \varepsilon\kappa\frac{k_x k_y}{|k|}\hat{h}(k_x,k_y), \tag{3}$$

where

$$\phi = \begin{matrix} +\pi/4 & (k_x \geq 0) \\ -\pi/4 & (k_x < 0) \end{matrix}, \tag{4}$$

and x is the downwind distance, y is the crosswind distance, ε is a dimensionless factor, κ is the von Karman constant (0.4), k is the wave number (with x and y components), $\hat{h}(k_x, k_y)$ is the Fourier Transform of the topography, z_k is

$$z_k = 2\sqrt{\frac{z_0}{l}|k^*|}, \tag{5}$$

K_0 is the modified Bessel function of zero order, K_1 is the modified Bessel function of first order, z_0 is the aerodynamic roughness length, l is a characteristic "inner layer" thickness given by

$$l\ln\left(\frac{l}{z_0}\right) = 2L\kappa^2, \tag{6}$$

k^* is the normalized wavenumber (i.e. kL) and L is the half length of the bedforms at the half-height position (Jackson and Hunt, 1975). In most applications of the J&H model, where the goal is to calculate the flow over an isolated hill of prescribed size and shape, L is assumed to be constant. In this paper, where the goal is to model flow over evolving bedforms with a range of sizes, L changes with each Fourier coefficient, i.e. $L=\pi/2k_x$. Because the J&H model is linear (and hence solutions can be superposed), L can be allowed to vary in this way. The value of ε, a measure of the "strength" of the perturbation, is given by

$$\varepsilon = \frac{\ln^2\left(\frac{L}{z_0}\right)}{\kappa\ln\left(\frac{l}{z_0}\right)} \tag{7}$$

The J&H flow model includes only one intrinsic length scale: the aerodynamic roughness length z_0. That is, for a given topography (i.e. the topography at a given time step in the bedform evolution model), $\hat{h}(k_x, k_y)$, L, and l are prescribed, and the nature of the flow over the topography, including the magnitude of the normalized bed shear stress variations, τ_{b1}, will depend only on the length scale z_0.

The effect of the aerodynamic roughness length on the magnitude of bed shear stress variation over sinusoidal bedforms is illustrated in

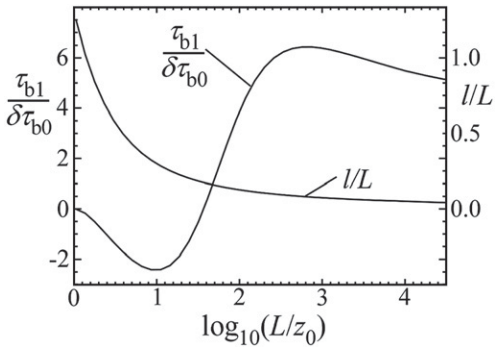

Fig. 3. Plots of normalized bed shear stress variations, $\tau_{b1}/\delta\tau_{b0}$, and normalized inner layer thickness, l/L, predicted by the Jackson and Hunt (1975) model versus the logarithm (base 10) of the ratio of the half height of the hill to the roughness length. This plot illustrates that the normalized bed shear stress variations reach a maximum when $L/z_0 \approx 500$.

Fig. 3. This figure plots the magnitude of the normalized bed shear stress variation, $\tau_{b1}/\delta\tau_{b0}$, as a function of the logarithm (base 10) of the ratio of the half-length of the bedforms to the roughness length, $\log_{10}(L/z_0)$. The normalized bed shear stress, τ_{b1}/τ_{b0}, is scaled in this plot to the tangent of the maximum slope angle, δ. Fig. 3 also plots the normalized inner layer thickness l/L computed by solving Eq. (4) iteratively. In order to interpret Fig. 3, let us first consider a sinusoidal bed of half length 10 cm and maximum slope 0.1. If the aerodynamic roughness length is relatively large (e.g., 1 mm, corresponding to $\log_{10}(L/z_0)=2$), for example, Fig. 3 shows that the value of $\tau_{b1}/\delta\tau_{b0}$ is approximately 4, hence $\tau_{b1}/\tau_{b0}=0.4$. This means that the bed shear stress will increase by approximately 40% near the crest of sinusoidal bedforms according to this model, and decrease by approximately 40% near the trough. At smaller roughness lengths, e.g., $z_0=0.1$ mm, the value of $\tau_{b1}/\delta\tau_{b0}$ increases to approximately 6. This increase in bed shear stress is associated with the fact that, for relatively small roughness lengths, the wind velocities interacting with the bedforms will be greater (due to the higher velocity gradients associated with smaller roughness lengths), hence the degree of flow compression/expansion will also be greater. At still smaller roughness lengths, however, e.g. $z_0=0.01$ mm, the value of $\tau_{b1}/\delta\tau_{b0}$ actually decreases to slightly more than 5. This decrease is associated with the increase in form drag and backpressure that limit near-surface wind velocities compared to the cases with lower L/z_0 ratios (Wood and Mason, 1993). The shape of this plot illustrates that, for a given topography, there is a certain value of z_0 that maximizes the variations in bed shear stress over sinusoidal bedforms. If the ratio L/z_0 is too low, the bed shear stress variations are small because the bedforms are too small to experience the high-velocity winds that occur far from the bed. If the ratio L/z_0 is too large, backpressure effects act to limit the bed shear stress. In between these two extremes, an optimal condition exists where the bedforms are tall enough (relative to the roughness length) to drive significant flow compression and expansion but not so tall that backpressure and form drag become a limiting factor. In addition to the magnitude of bed shear stress variations, the roughness length also controls the phase shift between the bed shear stress and the topography. For larger values of z_0, the maximum of bed shear stress is shifted further upwind from the bedform crest.

The J&H flow model is a linear model that is accurate to within a few percent only for maximum slopes less than approximately 0.2 (i.e. ≈10°). Because mature bedforms commonly attain slope angles close to or equal to the angle of repose, some modification to the J&H model is necessary in order to model the development of ripples and dunes. Schwammle and Herrmann (2004), for example, modified the bed shear stress predicted by the J&H model on the lee side of growing dunes using a geometric model for the region of flow separation. This approach neglects the effect of flow separation (and of drag-induced backpressure more generally) on the rest of the boundary layer. Consider the case of flow over steep ramps (forward and backward-facing), illustrated in Fig. 4. In the forward facing case, we can expect the normalized bed shear stress or speedup ratio above the ramp to increase with increasing ramp angle, at least for small angles. This is because flow lines converge as the flow moves over the step, causing higher velocity gradients and bed shear stresses. In the extreme case of a vertical step, however, the flow will stagnate behind the step and the speedup ratio will be lower than that of a flat surface. In that case, the stagnation zone in front of the step leads to a low shear stress because of the backpressure that develops behind the zone of stagnant flow. Between these two extreme cases, there must be some transition from increasing bed shear stress to decreasing bed shear stress as the ramp slope increases. The J&H model, however, predicts an increasing bed shear stress for all slopes. Although the J&H model does include the backpressure effects associated with gentle slopes, it is clear that the J&H model (or any other linear model) does not include the transition of increasing bed shear stresses to decreasing bed shear stresses as slope angle increases and nonlinear flow effects become dominant.

In order to quantify the nonlinear relationship between bed shear stresses and bed slope, I computed the boundary layer flow over forward- and backward-facing ramps of various inclinations using the Nonlinear Mixed Spectral Finite Difference Model (NLMSFD) of Xu et al. (1994). This model has been used successfully to quantify the nonlinear effects of flow separation on speedup ratios over sinusoidal topography (Ayotte and Hughes, 2004; Ayotte, 2008). The open circles in Fig. 4 represent the maximum bed shear stress on the inclined portion of the ramp predicted by the NLMSFD model, with a step height of 10 cm and a roughness length of 1 mm. These results indicate

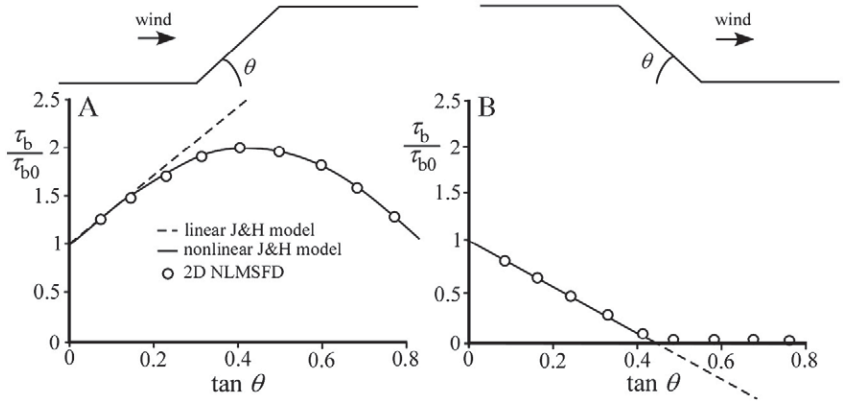

Fig. 4. Plots of peak normalized bed shear stress, τ_b/τ_{b0}, over (A) forward and (B) backward-facing steps according to the Jackson and Hunt model (dashed line), modified, nonlinear Jackson and Hunt model of this paper (solid curve, see text for details), and 2D Nonlinear Mixed Spectral Finite Difference (NLMSFD) model of Xu et al. (1994).

that the maximum bed shear stress on a forward facing ramp initially increases linearly with slope tan θ, following the prediction of the J&H model closely until tan $\theta \approx 0.2$. As tan θ increases, the bed shear stress reaches a maximum value at tan $\theta \approx 0.4$ and then decreases as backpressure becomes a dominant factor. In the backward-facing step case, the NLMSFD results follow the predictions of the J&H model closely until separation occurs at tan $\theta \approx 0.4$. At larger slopes, the bed shear stress remains close to zero in the nonlinear model, while the linear model predicts negative bed shear stresses.

The NLMSFD model is too computationally intensive to be run in 3D during each time step of the bedform evolution model. Therefore, some abstraction of the results of the NLMSFD model must be used. Results from the NLMSFD model suggest a way in which the J&H model can be corrected for nonlinear effects over steep topography. In this modified model, which I refer to as the "modified, nonlinear J&H model," the local bed shear stress predicted by the linear model, τ_b, is modified by the local slope in the downwind direction, $\partial h/\partial x$, according to a parabolic function:

$$\tau_{b,nl} = \tau_b\left(1-2\left(\frac{\partial h}{\partial x}\right)^2\right) \quad \text{if} \quad \frac{\partial h}{\partial x} > 0, \tag{8}$$

where the subscript nl refers to the nonlinear modification. Fig. 4 shows that Eq. (8) closely follows the trend observed in the NLMSFD results for the case of the forward-facing step. The precise shape of the nonlinear transition plotted in Fig. 4 and represented empirically by Eq. (8) will vary as a function of the shape of the step and the aerodynamic roughness length, however. As such, Eq. (8) is only an approximation based on representative NLMSFD results for flow over abrupt changes in slope. In the backward-facing ramp case, it is appropriate to modify the bed shear stress predicted by the linear model by making the stress equal to zero if the predicted value is less than zero, i.e.

$$\tau_{b,nl} = 0 \quad \text{if} \quad \tau_b < 0. \tag{9}$$

Eq. (9), which is not plotted in Fig. 4 because it follows the linear model until the bed shear stress is equal to zero and then follows the x axis at $\tau_b = 0$ for higher values of tan θ, closely follows the trend observed in the NLMSFD results for the case of a backward-facing step.

Once the bed shear stress is computed, the bedform evolution model computes the flux at each grid point, q_x, using the relationship

$$q_x = \begin{array}{ll} c\tau_b^{1/2}(\tau_b - \tau_{bt}) & \text{if} \quad \tau_b \geq \tau_{bt} \\ 0 & \text{if} \quad \tau_b < \tau_{bt} \end{array}, \tag{10}$$

where τ_{bt} is the threshold shear stress for entrainment and c is a coefficient that quantifies the bed erodibility and is primarily a function of grain size. The value of c is set to 1 in the model for simplicity. As a result, the units of time in the model are arbitrary. The threshold bed shear stress for entrainment, τ_{bt}, is given by

$$\tau_{bt} = \tau_{bt0}\frac{S_c + \frac{\partial h}{\partial x}}{S_c\sqrt{\left(\frac{\partial h}{\partial x}\right)^2 + 1}}, \tag{11}$$

where τ_{bt0} is the threshold bed shear stress for entrainment on a flat bed, given by

$$\tau_{bt0} = A^2(\rho_s - \rho)gD, \tag{12}$$

S_c is the tangent of the angle of repose (0.67), A is the entrainment coefficient (equal to 0.1 for air flow over a sandy bed), ρ_s is the sediment density, g is the acceleration due to gravity, and D is the grain size (Bagnold, 1936). The threshold shear stress over flat topography, τ_{bt0}, can be introduced into the model most simply by defining the threshold to be a ratio, α, of the applied shear stress over the initially flat topography, i.e. $\alpha = \tau_{bt0}/\tau_{b0}$. Topography influences sediment transport over bedforms in two separate ways. First, topographic variations cause flow compression and expansion that increase or decrease bed shear stress, as represented in the modified, nonlinear J&H model. Eq. (11) indicates that topography influences sediment transport through an additional mechanism, however. The local slope of the bed changes the threshold shear stress necessary to entrain sediment (e.g., less bed shear stress is required to entrain sediment from a lee slope due to the sloping geometry of the surface) (Howard, 1977; Hardisty and Whitehouse, 1988; Willetts and Rice, 1988; Iversen and Rasmussen, 1999). This additional topographic control on sediment transport has been neglected in recent bedform evolution models (e.g. Stam 1996, 1997; Schwammle and Herrmann, 2004) by assuming $\tau_{bt} >> \tau_{bt0}$.

The bedform evolution model of this paper integrates the boundary layer flow and sediment transport models described above with a modified version of Werner's (1995) bedform evolution model. In the model, all of the length scales in the problem are scaled to z_0. As such, the value of z_0 in the model is set to 1 and the height and spacing of bedforms produced by the model have units that are multiples of z_0. In this way, the model represents the feedbacks between topography, air flow, and erosion and deposition in a scale-independent way. To scale the bedform heights and spacings predicted by the model to actual units, one needs only to multiply the model predictions for height and spacing by a specific value of z_0.

In Werner's model, sand units are picked up at random and transported a unit distance l_s downwind. In the present model, sand units are entrained with a probability p_e that depends on the local flux q_x in the direction of the wind, with a coefficient p_0:

$$p_e = p_0 q_x. \tag{13}$$

Following downwind transport of the sand unit a distance l_s, the sand unit falls back to the bed with a probability p_d that also depends on flux according to:

$$p_d = p_0(1 - q_x) \tag{14}$$

Because Eqs. (13) and (14) relate the probabilities of entrainment and deposition linearly to q_x, the time-averaged flux in the model is proportional to q_x. The value of p_0 is chosen such that $p_e = 1 - p_d \approx 0$ on the lee sides of well-developed bedforms (i.e. in zones of flow recirculation where transport is predominantly by avalanching) and $p_e = 1 - p_d \approx 1$ on stoss sides. Since q_x varies from approximately 0 (in recirculation zones) to as high as 2.5 (on the stoss sides of mature bedforms), a value of p_0 between 0.3 and 0.4 is an appropriate default value. Finally, as in Werner's model, avalanching occurs if the entrainment or deposition of any sand unit causes an oversteepened condition (i.e. a local slope angle in excess of 33°), and the avalanching sand units are transported in the direction of steepest descent.

The bedform evolution model of this paper is fully defined with six parameters: N, the number of grid points in the x and y directions; Δx, the width of an individual grid point; Δh, the height of an individual sand unit; l_s, the displacement unit of each sand unit; p_0; and α. All of the length scales in the model are scaled to the fundamental length scale of the problem, z_0. For the model results presented here, I use $N = 256$, $\Delta x = 500 z_0$, $\Delta h = 25 z_0$, $l_s = \Delta x$, $p_0 = 0.33$, and $\alpha = 0$ unless otherwise noted. Time in the model is measured by the number of time steps normalized by the total number of grid points N^2. Varying the values of Δh, l_s, and/or p_0 in the model affects how quickly bedforms develop, but not the resulting geometry (height and spacing) of those bedforms. If the value of Δh is lowered, for example, the model exhibits smaller fluctuations in sediment transport, hence more time is required for the instability to develop. Varying Δx changes the model resolution but does not change the geometry of bedforms as long as individual bedforms are sufficiently well resolved.

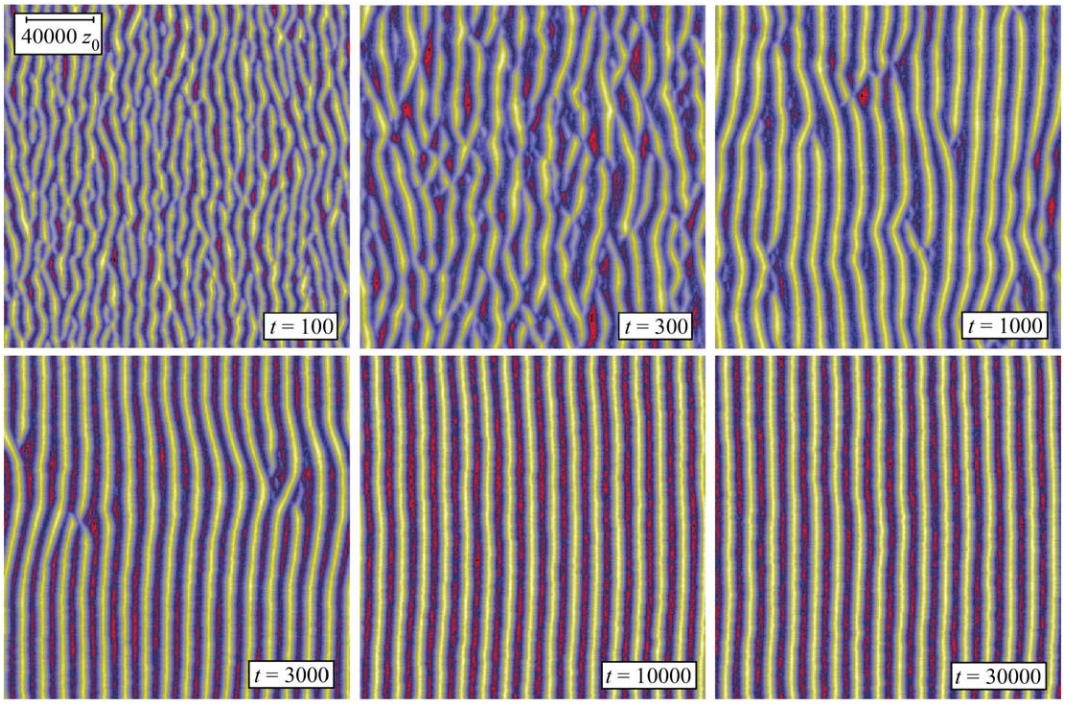

Fig. 5. Color maps of elevation predicted by the bedform evolution model with the linear Jackson and Hunt boundary layer flow model at $t = 100$, 300, 1000, 3000, 10,000, and 30,000 ($\times N^2$) time steps. In the model, bedform spacing and crest line length increase until a steady-state condition is achieved after $t \approx 1000 \times N^2$ time steps.

2.2. Model results

In order to determine the effects of the nonlinear relationship between windward speedup ratio and bed shear stress on bed slope, let's first consider a "control" model run with a version of the bedform evolution model that uses the linear J&H flow model. Parameters for this run are $N = 256$, $\Delta x = 1000 z_0$, $\Delta h = 50 z_0$, $l_s = \Delta x$, $p_0 = 0.33$, and $\alpha = 0$. Fig. 5 illustrates color maps of the surface topography predicted by this version of the bedform evolution model. A scale bar is included in the upper left corner of the figure and the wind direction is from left to right. Early on in the model run, narrowly-spaced bedforms are created with short crest lines and a high defect density. Over time, bedform height, spacing, and crest-line length all increase while defect density decreases. After $t \approx 1000 \times N^2$, the model achieves a steady-state condition in which there is no further growth in height or spacing. In steady state, the model predicts that bedform spacing is equal to approximately 10,000 times

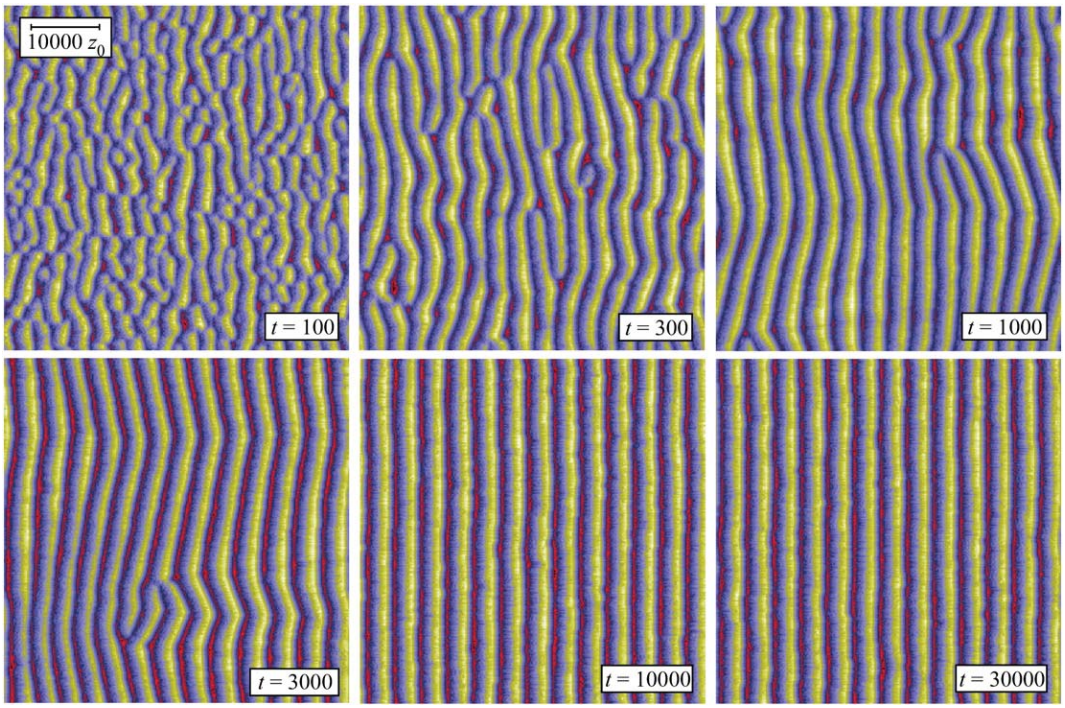

Fig. 6. Color maps of elevation predicted by the bedform evolution model with the modified (nonlinear) Jackson and Hunt boundary layer flow model at $t = 100$, 300, 1000, 3000, 10,000, and 30,000 ($\times N^2$) time steps. In the model, bedform spacing and crest line length increase until a steady-state condition is achieved after $t \approx 1000 \times N^2$ time steps.

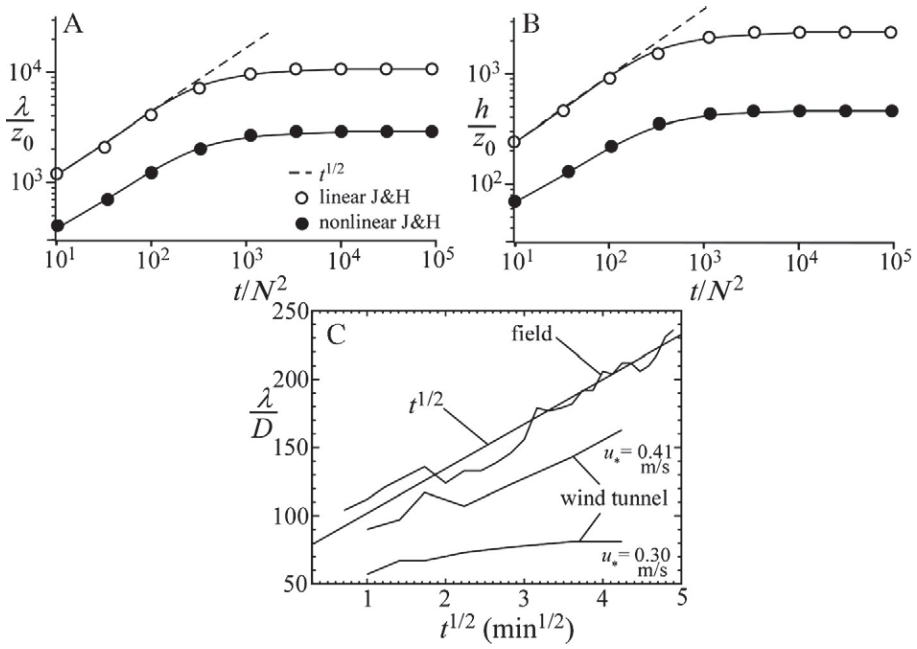

Fig. 7. Plot of (A) normalized spacing, λ/z_0, and (B) normalized height, h/z_0, versus time for the bedform evolution model with the linear Jackson and Hunt model (open circles) and the modified, nonlinear version (close circles) based on an average of ten simulations. Early in the model, height and spacing grow proportionately to the square root of time (dashed line), but eventually reach a steady-state condition in which height and spacing do not increase significantly with time. (C) Field and wind tunnel experiments on ripple formation showing that bedform spacing closely follows the square root relationship observed in the model for short time scales.

the roughness length ($\lambda \approx 10{,}000 z_0$) and bedform height is approximately 3000 times the roughness length ($h \approx 3000 z_0$.). This behavior is illustrated in Fig. 7, which shows that the spacing and height of bedforms both increase proportionately to the square root of time until a steady-state condition is achieved. The achievement of a steady-state condition in this model can best be understood as a balance between two competing effects that relate migration rate to bedform height. In Werner's (1995) model, bedform migration rate is inversely proportional to bedform height. Over time, smaller bedforms migrate faster than larger bedforms, causing bedforms to coalesce over time with no preferred length scale. Hence, bedform size increases as a power law over time with no maximum size. It should also be emphasized that the increase in bedform height and spacing in Werner's model continues even after all of the defects have been removed from the system. In contrast, bedform migration rate in this model is influenced by bedform height in two independent ways. As in Werner (1995), taller bedforms migrate more slowly due to the increase in cross-sectional surface-area-to-volume ratio with increasing height (which causes migration rate to be inversely proportional to height if slopes are constant). Taller bedforms, however, are subject to greater speedup ratios and bed shear stresses for a given width (within a certain range of λ/z_0), causing taller bedforms to migrate faster than they do in Werner's model. This boundary layer flow effect does not only depend on the height of the migrating bedform, but also on the heights of bedforms upwind and downwind via boundary-layer interactions. The existence of a steady-state height and spacing in the model is related to a competition between these two opposing effects. As with Werner's (1995) model, however, this model is also limited in that it predicts symmetric bedform profiles (i.e. both the stoss and lee slopes achieve angles close to the angle of repose). Including a finite threshold shear stress (i.e. $\alpha > 0$) in the model does not measurably change the size of the resulting bedforms.

Figs. 6 and 7 illustrate the corresponding results for the bedform evolution model with modified, nonlinear J&H flow. The relationship between bedform spacing and time in this version of the model is broadly similar to that of the linear model illustrated in Fig. 5. Over time, bedform height, spacing, and crest-line length all increase while defect density decreases. After $t \approx 1000 \times N^2$, this model also reaches a steady-state condition. In contrast to the linear J&H model, however, bedforms in this model are asymmetric, with slope angles of ≈20° on the stoss slopes and close to 33° on the lee slopes (Fig. 8). In steady state, this model predicts that bedform spacing is equal to approximately 3000 times the roughness length ($\lambda \approx 3000 z_0$) and bedform height is approximately 600 times the roughness length ($h \approx 600 z_0$). This version of the bedform evolution model is clearly the preferred version, both because it incorporates a flow model with more realistic nonlinear effects and because it leads asymmetric bedform topographic profiles similar to those observed in nature (Fig. 8). Including a finite threshold shear stress (i.e. $\alpha > 0$) in this version of the model also does not measurably change the size of the resulting bedforms, but the shape of the bedforms do change. The model predicts lower stoss slopes and bedform aspect ratios with higher values of α.

2.3. Application to ripples

Available data on the growth of ripple spacing versus time is consistent with the square root dependence on time observed in the model prior to steady state. Fig. 7C illustrates ripple spacing data from

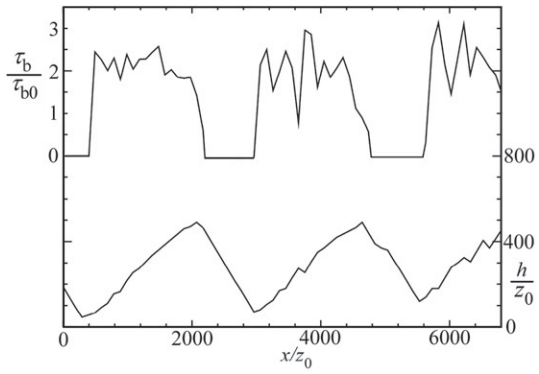

Fig. 8. Plot of normalized bed shear stress and topography as a function of downwind distance predicted by the bedform evolution model with the modified, nonlinear Jackson and Hunt flow model. Bedforms are asymmetric, with maximum slope angles on the stoss side of ≈15° and maximum angles on the lee side of 33°.

a 25 minute field experiment of ripple formation and two wind tunnel experiments performed at different shear velocities. Werner and Gillespie (1993) used this data to support a logarithmic increase in ripple spacing versus time, but they fitted their model to only a portion of the data. Fig. 7C shows that, in the case of the field experiment and the wind tunnel experiment with high shear velocity (i.e. u_*=0.41 m s^{-1}), the entire dataset closely follows the $t^{1/2}$ dependence, consistent with the model of this paper and with the cellular automaton model of Werner (1995). The field and laboratory measurements were acquired over too short a duration to document the transition to steady state, however. The results of the wind tunnel experiment performed at lower shear velocity (i.e. u_*=0.30 m s^{-1}) is not consistent with a square root dependence on time. This could be due to a transition to steady state. The limited resolution of the data, however, makes it difficult to reach any firm conclusion.

Next we evaluate the model prediction for the steady-state spacing of ripples formed on an initially flat surface. On a flat surface with active saltation, the aerodynamic roughness length is a function of the grain size and the excess shear velocity. Using measured values of z_0, D, and u_* from the literature, Sherman (1992) proposed the following expression:

$$z_0 = \frac{D}{15} + C_m \frac{(u_* - u_{*t})^2}{g} \tag{15}$$

where C_m is an empirical, dimensionless parameter and

$$u_{*t} = A\sqrt{\frac{\rho_s - \rho}{\rho} gD} \tag{16}$$

In the first term on the right side of Eq. (13), grain size influences roughness because grains are the discrete units from which the bed is composed and larger grains produce rougher microtopography and hence greater drag on the boundary layer whether or not saltation is occurring. During saltation (i.e. when $u_* - u_{*t} > 0$), an additional "saltation-induced" roughness occurs, represented by the second term on the right side of Eq. (15). The magnitude of this effect increases with the excess shear velocity, because higher values of excess shear velocity cause greater saltation. Sherman (1992) constrained the value of C_m to be 0.025 from 99 data points, the large majority of which were measured in wind tunnels. More recently, Sherman and Farrell (2008) used an analysis of an expanded dataset of 291 data points to propose a value of C_m=0.132 for field conditions. Sherman and Farrell (2008) documented that measurements of z_0 from wind tunnels are, on average, approximately an order of magnitude lower than those measured in the field, due to the effects of flow confinement in wind tunnels. This is the reason why the value for C_m in field conditions (0.132) is so much larger than the originally-proposed value (0.025).

Eq. (15), together with the fundamental scaling of bedform height and spacing to roughness length predicted by the bedform evolution model of this paper, provides the technical basis for predicting the dependence of ripple spacing on grain size and shear velocity in the field (Sharp, 1963; Wilson, 1972) and in the laboratory (Walker, 1981; Andreotti et al., 2006). It should be noted that natural sand beds have a range of grain sizes and it is possible that coarser grains have greater influence on aerodynamic roughness than median-sized grains. For this reason, many field studies of the granulometric control of ripple and dune spacing have used the grain size of the coarsest 20th percentile (e.g. Wilson, 1972; Lancaster, 1988) instead of the mean grain diameter, D, when testing the granulometric control of bedform size. Here we will use Eq. (15) to estimate the roughness length during ripple formation for comparison to measured data, even if the measured data report P_{20} values, bearing in mind that values of D may be significantly lower than values of P_{20}.

Fig. 9A plots the predictions of the model for a range of values of the grain diameter and shear velocity, along with field measurements of ripple spacing verses grain size from the Saharan Sand Seas (Wilson, 1972) and from Kelso Dunes, California (Sharp, 1963). Measurements of ripple spacing in wind tunnels (not plotted) are similar to the values measured by Sharp (1963), e.g. Walker (1981) measured ripples from 5–10 cm in spacing for median grain sizes of 0.2–0.8 mm. Fig. 9A plots the ripple spacing predicted by the model (i.e. $\lambda \approx 3000 z_0$), using Eq. (15) with C_m=0.132 (i.e. field conditions) to estimate z_0 as function of D or P_{20} and $u_* - u_{*t}$, for three excess shear velocity values: $u_* - u_{*t} \geq 0$, 0.1, and 0.2 m s^{-1}. For conditions just above the transport threshold, the model predicts ripple spacings very close to the values measured by Sharp (1963), e.g. λ=4–8 cm for D=0.25–0.5 mm and on the low end of the values reported by Wilson (1972). As the excess shear velocity increases, the predicted ripple spacing increases nonlinearly according to Eq. (15). The dependence of ripple spacing on excess shear velocity for a fixed grain size has been investigated by Walker (1981) and Andreotti et al. (2006). Both studies document a nonlinear increase in ripple spacing with excess shear velocity, as predicted by the model. It should be noted that the sensitive dependence of ripple spacing on excess shear velocity

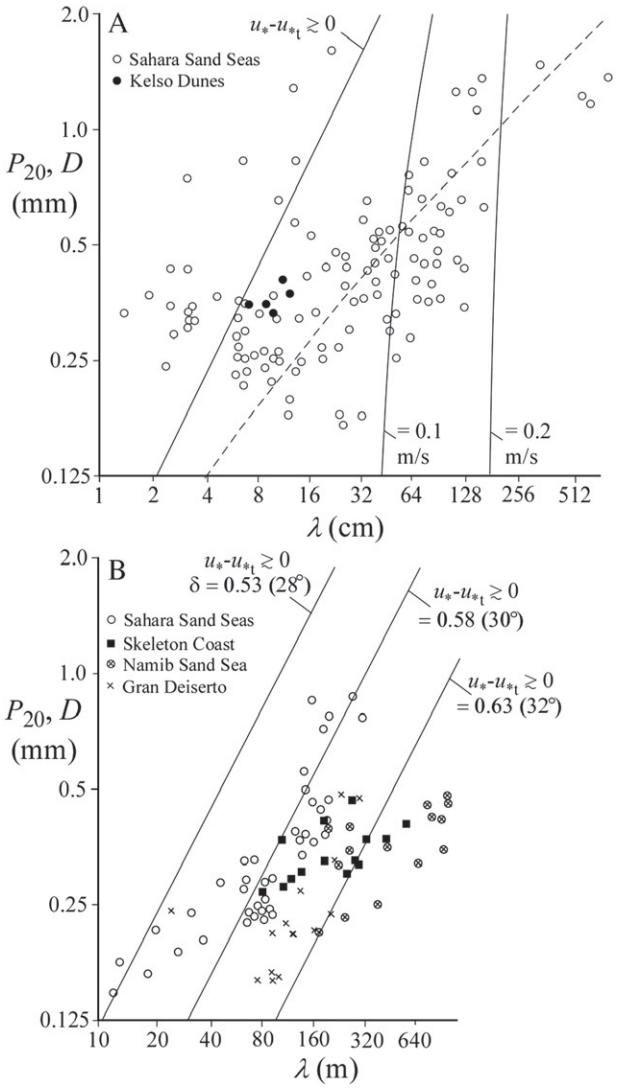

Fig. 9. Plots of P_{20} and D versus bedform spacing for (A) ripples and (B) dunes. (A) Data from Wilson (1972) (P_{20} reported, open circles) and Sharp (1963) (D reported, closed circles). Solid curves represent model predictions assuming no positive correlation between grain size and excess shear velocity. Dashed curve represents model prediction assuming a linear correlation between grain size and excess shear velocity. (B) Data from Wilson (1972) (P_{20} reported, open circles) and Lancaster (1988) (P_{20} reported, all other symbols). In addition to grain size and shear velocity, predicted dune spacing is a sensitive function of maximum ripple slope, δ.

predicted by the model and illustrated in Fig. 9A applies only to field conditions. In wind tunnels, the value of C_m is approximately an order of magnitude lower (Sherman and Farrell, 2008; but C_m will likely vary with the size of the wind tunnel), and hence the model predictions for ripple spacing in wind tunnels implies that larger excess shear velocities are required to achieve the same increase in ripple spacing compared to field conditions.

It should be noted that Eq. (15) is only one possible model of saltation-induced roughness. Eq. (15) assumes that saltation-induced roughness (i.e. the second term on the right side of Eq. (15)) is not an explicit function of grain size (i.e. except for the grain size dependence implicit in u_{*t}). For a given excess shear velocity, larger grains may exert more drag on the flow compared to smaller grains. In Sherman's (1992) analysis, he noted that a multivariate analysis of measured z_0 values versus both D and u_*-u_{*t} revealed that saltation-induced roughness does, in fact, depend on grain size, but the data were inconclusive as to what particular form that dependence takes. One difficulty with determining the grain-size dependence of saltation-induced roughness is the relatively narrow range of grain sizes over which field and wind tunnel experiments have been performed. In Sherman's (1992) compilation, a large majority of measurements were collected for grain sizes between 0.2 and 0.4 mm, i.e. much smaller than the range of grain sizes studied by Wilson (1972).

Another complicating factor to consider is the potential correlation of grain size and excess shear velocity in the field. The model predictions plotted in Fig. 9A assume that grain size and shear velocity are independent variables. That is, each curve shows the trend in ripple spacing predicted by the model for different values of P_{20} or D assuming a uniform value of u_*-u_{*t} across the study area. In the field, however, it is possible that grain size and excess shear velocity are positively correlated. For example, areas characterized by higher average excess shear velocity conditions could transport a greater proportion of fine sand, leaving behind a locally coarse lag. As an illustration of the implications of such a correlation for ripple spacing, let's assume that grain size and excess shear velocity are linearly correlated in the field such that:

$$D = a(u_*-u_{*t}) \tag{17}$$

where a is an empirical coefficient that varies from one dune field to the next but is constant within a given dune field. The dashed curve in Fig. 9A illustrates the ripple spacing predicted using Eq. (17) substituted into Eq. (15), with $a=0.00015$ s. The correlation represented by Eq. (17) is purely hypothetical, but it illustrates one hypothesis for the nonlinear grain size control documented in the Sahara by Wilson (1972). Similarly, if the saltation-induced roughness is an increasing function of grain size, the model prediction for ripple spacing will also become a nonlinear function of grain size similar to the dashed curve in Fig. 9A. Although significant uncertainties exist in quantifying saltation-induced roughness and potential correlations between grain size and excess shear velocity in the field, the model predicts values for ripple spacing that are similar to the range of values observed in the field and in wind tunnel experiments. In addition, the model reproduces the positive correlation between grain size, excess shear velocity, and ripple spacing observed in both field and wind tunnel measurements.

2.4. Application to transverse dunes

Once ripples form in areas with abundant sand supply, they become the dominant roughness elements on the surface, thus creating a larger effective roughness length. The scale-independent nature of the bedform evolution model in this paper suggests that the creation of a new, larger, effective roughness length caused by ripple formation should trigger the same bedform instability that formed ripples at a larger spatial scale. This conceptual model suggests a possible genetic linkage between ripples and dunes.

To apply this model to quantifying the spacing of dunes, it is necessary to estimate the effective aerodynamic roughness length of a rippled surface based on the roughness length of the initially-flat surface and the ripple morphology. The oceanographic literature provides the necessary relationship to make this calculation (i.e. Jacobs, 1989). In the oceanographic case, wind-generated water waves are the roughness elements analogous to ripples in the eolian case. Jacobs' (1989) analysis predicts that the effective aerodynamic roughness length, z_e, over sinusoidal topography is given by

$$\frac{z_e}{z_0} = \exp\left(\frac{1}{2}\left(\delta \ln\left(\frac{L}{z_0}\right)\right)^2\right) \tag{18}$$

where z_0 is the roughness length of the originally-flat surface (calculated in Eq. (15)), L is the half-length of the ripples at the half-height position, and δ is the maximum slope of ripples. Eq. (18) is only accurate to approximately an order of magnitude, however, because ripples are not sinusoidal and the predictions of Eq. (18) are very sensitive to the maximum ripple slope, δ. Conceptually, the sensitivity of z_e/z_0 to δ is a consequence of the fact that, in the vicinity of the threshold slope for flow separation, small changes in the bed slope can result in large changes in the structure of boundary layer flow. Computational fluid dynamic (CFD) modeling of boundary layer flows over ripples of various shapes and sizes will be needed to more precisely quantify the value of z_e/z_0 for natural ripples. It should be emphasized that the "new" roughness length caused by ripple formation does not eliminate the roughness length of the initially flat surface. Rather, the velocity profile above a surface with two dominant scales of roughness is a composite velocity profile characterized by two roughness lengths, one that characterizes flow very close to the bed and one that characterizes flow at a larger spatial scale. It is the roughness length associated with this larger spatial scale that controls the flow convergence/expansion over dunes as they develop.

Fig. 9B plots measured spacings of transverse dunes from the Sahara Sand Seas (Wilson, 1972) and from the Skeleton Coast, Namib Sand Sea, and Gran Desierto (Lancaster, 1988). In focusing on these datasets I have intentionally left out dunes formed in areas of limited sand supply (i.e. barchan, star, and longitundal dunes) for the reason that the aerodynamic roughness length over dunes formed in areas of limited sand supply will be controlled, in part, by the roughness elements of interdune or sand-free areas rather than by grain size. Taken collectively, dune spacing in the Wilson and Lancaster datasets show a weak correlation with grain size. Within individual dune fields, however, the correlation is much stronger. The solid curves in Fig. 9B correspond to the model prediction for $u_*-u_{*t}\geq 0$, $L/z_0=750$ (i.e. assuming the model prediction for ripple spacing, i.e. $\lambda\approx 3000z_0$), and several values for the maximum ripple slope: $\delta=0.53$ (i.e. the tangent of 28°), 0.58 (30°), and 0.63 (32°). Fig. 9B illustrate the extreme sensitivity of the model predictions to the maximum ripple slope, δ. Limited data exist for the maximum slope of ripples, but Sharp (1963) and Werner et al. (1986) put the range at between 25° and 30°. According to the model predictions, dunes formed with maximum ripple slopes of 28° have spacing values on the low side of measured values, while dunes formed with steep ripples (up to a maximum value of 33°) yield dunes with spacing values equivalent to the largest measured dunes. Although the model results are only illustrated for a single value of u_*-u_{*t}, the model predicts that dune spacing will increase with increasing u_*-u_{*t}, in the same proportion as it does for ripple spacing in Fig. 9A. As such, an increase in excess shear velocity *or* maximum ripple slope results in larger dunes according to this model. The sensitivity of dune spacing to the maximum ripple slope provides one possible explanation for the variation in dune spacing between dune fields. Similarly, variations in shear velocity from one

dune field to another may also be responsible for variations in dune spacing between dune fields.

3. Discussion

The model of this paper clearly shows that ripples and dunes reach a steady-state condition in which they migrate downwind without further growth. Using a broadly similar model of transverse dune formation (i.e. a mass conservative model of coupled boundary layer flow with erosion, deposition and avalanching), however, Schwammle and Herrmann (2004) concluded that bedform height and spacing increased proportionately to the square root of time indefinitely. This discrepancy is explained by the fact that Schwammle and Herrmann (2004) plotted their results over only one order of magnitude of time. Fig. 7 illustrates that the initial period of bedform growth takes place over two orders of magnitude in time prior to the attainment of steady state.

The model results of this paper provide a preliminary process-based understanding of the grain size and wind velocity controls on the height and spacing of transverse eolian bedforms documented by Sharp (1963) and Walker (1981) for ripples, and Wilson (1972) and Lancaster (1988) for dunes in areas of abundant sand supply. The basis for this understanding is the numerical model prediction that the steady-state height and spacing of transverse eolian bedforms scales with the aerodynamic roughness length. In the model, ripples form from a flat bed with a height and spacing that increase with increasing grain size and excess shear velocity, both of which control the aerodynamic roughness length z_0 via Sherman's relation (i.e. Eq. (15)). Once ripples form, they become the new dominant roughness element on the surface. The effective roughness length of the rippled surface triggers bedform creation at a larger scale, thus creating dunes. As a result, the spacing of dunes is also controlled by grain size and excess shear velocity in this model, because the effective roughness length of the rippled surface (i.e. Eq. (18)) is larger than the original roughness length of the flat surface by a constant scaling factor that depends on the detailed shape (i.e. maximum slope) of the ripples. It should be noted, however, that dune formation in nature and in the model does not require the existence of ripples. Instead, dunes can form on any surface with an aerodynamic roughness length similar to that of ripples, including gravel surfaces. For example, dunes are predicted to form in the model with a spacing of approximately 100 m if the aerodynamic roughness length is approximately 1/3000 of that value, i.e. 3 cm. Roughness lengths of this value are broadly consistent with roughness lengths of gravel surfaces without ripples.

Wilson (1972) argued that megadunes represent a distinctly different type of bedform from dunes, based on the fact that dunes and megadunes are distinct populations in his granulometric plot. Recent research, however, suggests that megadunes are composite bedforms that represent multiple periods of construction (e.g. Stokes and Bray, 2005; Bristow et al., 2007). The model of this paper, with its dependence on excess shear velocity, is broadly consistent with this composite-bedform hypothesis for megadunes. Specifically, megadunes with spacings of 1–3 km are predicted to form in the model under conditions of high average shear velocity (e.g. $u_* - u_{*t} = 0.25$–0.4). Such conditions may have occurred over sufficiently long time periods during glacial climates for megadunes to form. According to this hypothesis, present conditions may be characterized by lower effective excess shear velocities. As a result, the dune-forming instability may be concentrated at smaller spatial scales than those that were active when megadunes formed.

Although the numerical model of this paper represents the best compromise between computational speed and realistic boundary layer flow necessary to model ripples and dunes as they evolve over many time steps, it is important to emphasize that a complete numerical model for eolian bedforms will require a model that more accurately quantifies how steep slopes and flow separation impact the entire boundary layer. In this paper, I incorporated the nonlinear effects of flow around steep topography by a local slope-dependent correction term. This approach provides, I believe, the best compromise between computational speed and model realism given that more complex turbulence models are computationally far too intensive to be coupled to complex, evolving bed topography in 3D. A complete model for bedforms will also require a model that includes multiple grain sizes and the role of sorting on bedform morphology as bedforms develop.

Acknowledgements

This study was partially funded by the Army Research Office Terrestrial Sciences Program, grant W911NF-04-1-0266. I wish to thank Nick Lancaster and Gary Kocurek for critical reviews of an earlier draft of the manuscript that led to a significantly improved paper. I also wish to thank Takashi Oguchi for his careful editing of the manuscript.

References

Anderson, R.S., 1987. A theoretical model for aeolian impact ripples. Sedimentology 34, 943–956.
Anderson, R.S., Bunas, K.L., 1993. Grain size segregation and stratigraphy in aeolian ripples modelled with a cellular automaton. Nature 365, 740–743.
Andreotti, B., Claudin, P., Pouliquen, O., 2006. Aeolian sand ripples: experiment study of fully developed states. Physical Review Letters 96 (L028001). doi:10.1103/PhysRevLett.96.028001.
Ayotte, K.W., 2008. Computational modeling for wind energy assessment. Journal of Wind Engineering and Industrial Aerodynamics 96 (10–11), 1571–1590.
Ayotte, K.W., Hughes, D.E., 2004. Observations of boundary-layer wind-tunnel flow over isolated ridges of varying steepness and roughness. Boundary Layer Meteorology 112, 525–556.
Baas, A.C.W., 2007. Complex systems in aeolian geomorphology. Geomorphology 91, 311–331.
Bagnold, R.A., 1936. The movement of desert sand. Proceedings of the Royal Society of London Series A 157, 594–620.
Bagnold, R.A., 1941. The Physics of Blown Sand and Desert Dunes. Methuen & Co., London, United Kingdom.
Bristow, C.S., Duller, G.A.T., Lancaster, N., 2007. Age and dynamics of linear dunes in the Namib Desert. Geology 35, 555–558.
Elbelrhiti, H., Andreotti, B., Claudin, P., 2008. Barchan dune corridors: field characterization and investigation of control parameters. Journal of Geophysical Research, Earth Surface 113 (F02S15). doi:10.1029/2007JF000767.
Folk, R.L., 1976. Rollers and ripples in sand, streams, and sky: rhythmic alteration of transverse and longitudinal vortices in three orders. Sedimentology 23, 649–669.
Hanna, S.R., 1969. The formation of longitudinal sand dunes by large helical eddies in the atmosphere. Journal of Applied Meteorology 8, 874–883.
Hardisty, J., Whitehouse, K.J.S., 1988. Evidence for a new sand transport process from experiments on Saharan dunes. Nature 332, 532–534.
Howard, A.D., 1977. Effect of slope on the threshold of motion and its application to orientation of wind ripples. Geological Society of America Bulletin 88, 853–856.
Howard, A.D., Morton, J.B., Gad-El-Hak, M., Pierce, D.B., 1989. Sand transport model of barchan dune equilibrium. Sedimentology 25, 307–338.
Iversen, J.D., Rasmussen, K.R., 1999. The effect of wind speed and bed slope on sand transport. Sedimentology 46, 723–731.
Jacobs, S.J., 1989. Effective roughness length for turbulent flow over a wavy surface. Journal of Physical Oceanography 19, 998–1010.
Jackson, P.S., Hunt, J.C.R., 1975. Turbulent wind flow over a low hill. Quarterly Journal of the Royal Meteorological Society 101, 929–955.
Lancaster, N., 1988. The development of large aeolian bedforms. Sedimentary Geology 55, 69–89.
Lancaster, N., 1996. The role of field experiments in studies of dune dynamics and morphology. Annals of Arid Zone 35, 171–186.
Mason, P.J., Sykes, R.I., 1979. Flow over an isolated hill of moderate slope. Quarterly Journal of the Royal Meteorological Society 105, 383–395.
Mitha, S., Tran, M.Q., Werner, B.T., Haff, P.K., 1986. The grain-bed impact process in eolian saltation. Acta Mechanica 63, 267–278.
Momiji, H., Carretero-Gonzalez, R., Bishop, S.R., Warren, A.W., 2000. Simulation of the effect of wind speedup in the formation of transverse dune fields. Earth Surface Processes and Landforms 25, 905–918.
Ould Ahmedou, D., Ould Mahfoudh, A., Dupont, P., Ould El Moctar, A., Valance, A., Rasmussen, K.R., 2007. Barchan dune mobility in Mauritania related to dune and interdune sand fluxes. Journal of Geophysical Research, Earth Surface 112 (F02106). doi:10.1029/2006JF000500.
Schwammle, V., Herrmann, H.J., 2004. Modelling transverse dunes. Earth Surface Processes and Landforms 29, 769–784.
Seppala, M., Linde, K., 1978. Wind tunnel studies of ripple formation. Geografiska Annaler 60, 29–42.
Sharp, R.P., 1963. Wind ripples. Journal of Geology 71, 617–636.

Sherman, D.J., 1992. An equilibrium relationship for shear velocity and apparent roughness length in aeolian saltation. Geomorphology 5, 419–431.
Sherman, D.J., Farrell, E.J., 2008. Aerodynamic roughness length over movable beds: comparison of wind tunnel and field data. Journal of Geophysical Research 113 (F02S08). doi:10.1029/2007JF000784.
Stam, J.M.T., 1996. Migration and growth of aeolian bedforms. Mathematical Geology 28, 519–536.
Stam, J.M.T., 1997. On the modeling of two-dimensional aeolian dunes. Sedimentology 44, 127–141.
Stokes, S., Bray, H.E., 2005. Late Pleistocene eolian history of the Liwa region, Arabian Peninsula. Geological Society of America Bulletin 117, 1466–1480.
Van Dijk, P.M., Arens, S.M., Van Boxel, J.H., 1999. Aeolian processes across transverse dunes. II. Modeling the sediment transport and profile development. Earth Surface Processes and Landforms 24, 319–333.
Walker, J.D., 1981. An experimental study of wind ripples. M.S. Thesis, Massachusetts Institute of Technology, Cambridge, MA, 145 pp.
Wasson, R.J., Hyde, R., 1983. A test of the granulometric control of desert dune geometry. Earth Surface Processes and Landforms 8, 301–312.
Weng, W.S., Hunt, J.C.R., Carruthers, D.J., Warren, A., Wiggs, G.F.S., Livingstone, I., Castro, I., 1991. Air flow and sand transport over sand-dunes. Acta Mechanica 2, 1–22.
Werner, B.T., 1995. Eolian dunes: computer simulations and attractor interpretation. Geology 23, 1107–1110.
Werner, B.T., Gillespie, D.T., 1993. Fundamentally discrete stochastic model for wind ripple dynamics. Physical Review Letters 71, 3230–3233.
Werner, B.T., Kocurek, G., 1997. Bed-form dynamics: does the tail wag the dog? Geology 25, 771–774.
Werner, B.T., Kocurek, G., 1999. Bedform spacing from defect dynamics. Geology 27, 727–730.
Werner, B.T., Haff, P.K., Livi, R.P., Anderson, R.S., 1986. Measurement of eolian sand ripple cross-sectional shapes. Geology 14, 743–745.
Willetts, B.B., Rice, M.A., 1988. Effect of bedslope on desert sand transport. Nature 334, 302.
Wilson, I.G., 1972. Aeolian bedforms: their development and origins. Sedimentology 19, 173–210.
Wippermann, F., Gross, G., 1986. The wind-induced shaping and migration of an isolated dune: a numerical experiment. Boundary Layer Meteorology 36, 319–334.
Wood, N., Mason, P., 1993. The pressure force induced by neutral, turbulent flow over low hills. Quarterly Journal of the Royal Meteorological Society 119, 1233–1267.
Xu, D., Ayotte, K.W., Taylor, P.A., 1994. Development of a non-linear mixed spectral finite difference model for turbulent boundary layer flow over topography. Boundary-Layer Meteorology 70, 341–367.